Synchronverter Coupled to a Lithium-Ion Bank for Grid Frequency and Voltage Supports and Controlled Charge-Discharge

Guilherme Penha da Silva Junior[a], Luciano Sales Barros[b] and Camila Mara Vital Barros[b]

[a] Federal University of Rio Grande do Norte, RN, Brazil
[b] Federal University of Paraiba, PB, Brazil

ARTICLE INFO

Keywords:
Synchronverter, lithium-ion battery, voltage and frequency support, battery charge-discharge control.

ABSTRACT

Many control strategies for grid-interfacing voltage source inverter (VSI) of distributed generation (DG) units have been reported for grid support, among them virtual synchronous machine (VSM) techniques, in particular the Synchronverter which has the ability to operate in voltage and frequency support mode, in active and reactive power control mode, in synthetic inertia and in conventional grid-side control of DG. The VSM-based VSI has its support capacity expanded by battery energy storage systems (BESS). In this work it proposes the Synchronverter to control a lithium-ion BESS connected to DC-bus of DG seeking grid frequency and voltage support. Since Synchronverter allows the conventional grid-side control which allows bi-directional flow, BESS charge-discharge is controlled without using DC/DC converter. Simulation results demonstrate the effectiveness of the Synchronverter for both of support and change-discharge control.

1. Introduction

The VSI used by renewable energy sources (RES) for grid integration is typically operated as controlled current source in "grid following" [10]. These VSIs have fast response and almost no moment of inertia; besides that, they cannot provide connection bus voltage control. Thus, it is difficult to provide necessary frequency and voltage supports for the grid [7]. Aiming to overcome these limitations, research is being conducted in order to enable VSI to participate of control and mitigation of low frequency and voltage oscillations of the grid [20].

The concept of VSM has been proposed as a possible solution to stability concerns, and so a VSI presents a “grid forming” control mode to improve behavior from a grid perspective [2][23][18][12]. The VSI controlled by VSM behaves like a synchronous generator (SG) and therefore can potentially be used to change system inertia and to voltage control [10].

There are several study groups that have developed the VSM concept: the VSYNC project (the project formed by several European companies and universities) [18],[6]; the ISE Laboratory in Osaka University in Japan [12],[5]; the Institute of Electrical Power Eng. (IEPE) in Germany [2],[3]; and the Synchronverter technique developed by [23].

In [17], performance tests were presented for the above mentioned VSM topologies. It was observed that the Synchronverter topology presented advantages over the other VSM topologies, showing itself as a promising solution to problems related to high integration of RES to the grid. It has made possible to operate as generator/motor with controlled active and reactive powers [15]. Also, the powers can be automatically shared using the well-known frequency and voltage-drooping mechanisms [14], acting in maintaining grid stability [11]. Moreover, the Synchronverter can provide virtual inertia to improve frequency stability, the same way as a conventional SG. This event slows down the tendency of decreasing inertia of the grid due to the high penetration of RES [24]. It is also capable of operating in a similar mode to conventional grid-side control (grid following), in which the active power is controlled based on the DC-bus voltage [16]. Another advantage is that the Synchronverter can automatically synchronize itself with the grid without using a phase-locked loop (PLL) [24]. The advantage is avoiding PLLs which are inherently nonlinear, so it is extremely difficult and time-consuming to tune adjustments to established parameters in order to obtain satisfactory performance [21].

In turn, BESS can be connected to the DC-bus of RES VSI since battery can supply lack of energy or store excess of energy from the grid, potentiating the use of VSM. In [13], the Synchronverter was used on a photovoltaic system whose the DC-bus is connected to a battery bank via a DC/DC converter to provide an uninterrupted supply even with irradiation and climatic changes. The battery works as an ancillary service to the PV system. Further, the behavior of the synchronverter under various voltage and frequency variations is analyzed.

In this paper it proposes to connect the BESS in parallel to DC-bus and control its charge-discharge without using the DC/DC converter but through the conventional grid-side control realized by Synchronverter, seeking to reduce the complexity of the control and the cost of the system. The proposed scheme uses converters in the back-to-back configuration, where the source-side converter is connected to the RES (wind or photovoltaic) and the grid-side converter is the Synchronverter, as it is shown in Fig. 1.

Therefore, the contributions of this work are supposed to be:

- Frequency support, active power regulation and syn-

*Corresponding author
gpsilvajr@gmail.com (G.P.d.S. Junior); lsalesbarros@ci.ufpb.br (L.S. Barros); cmaravb@gmail.com (C.M.V. Barros)
ORCID(s):

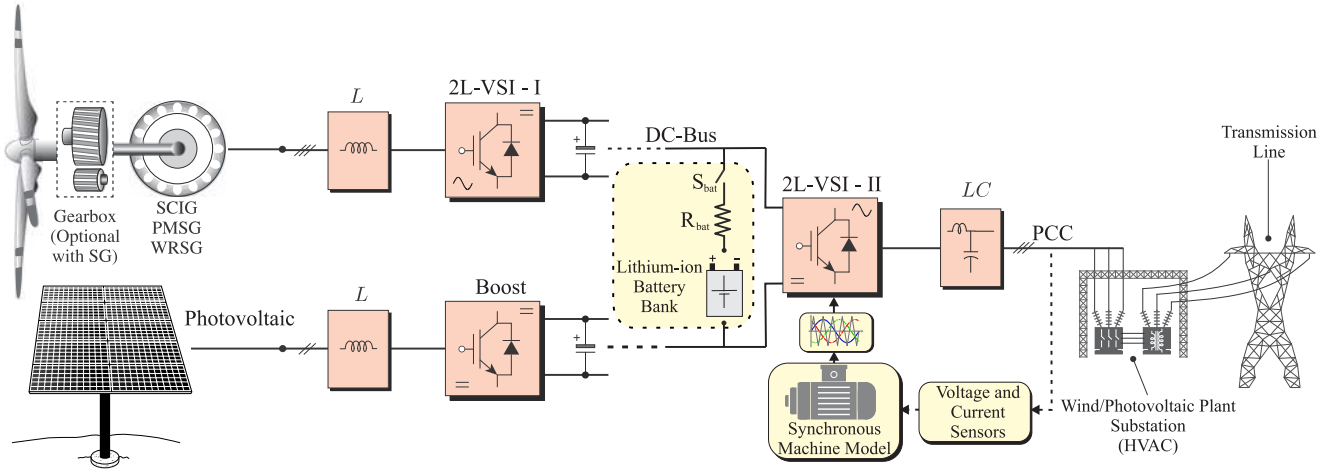

Figure 1: Proposed topology schematic. Own authorship, note: wind turbine, transformer and transmission line, adapted from [19].

thetic inertia, where the battery bank is able to self-charge without utilizing the DC/DC converter;

- Voltage support and regulation of reactive power to maintaining the voltage stability of the grid.

In order to test the proposed system performance, computer simulations are realized with the BESS represented by a model of a real lithium-ion battery. The VSI-I is controlled via conventional source-side control. The grid is represented by an infinite bus and an equivalent series impedance.

The remainder of the paper is organized as follow: Section II discusses the fundamentals of Synchronverter; Section III presents the model of the real lithium-ion BESS; Section IV presents the operation modes of the Synchronverter; Section V presents the simulations of case studies; and the Conclusions are given in Section VI.

2. Synchronverter

In this section, the details about how to implement a VSI as a Synchronverter will be described, as proposed in [22]. The structure of the Synchronverter can be divided into two parts: a control circuit and a power circuit.

2.1. Control Circuit

For VSI to have a similar behavior to a SG it is necessary to use second order mathematical model of the SG for the development of a control algorithm implemented for the VSI.

2.1.1. Electric Model

The synchronous generator has three windings in the armature (stator) and one winding in the rotor. The schematic sketch of the windings of the three-phase cylindrical rotor synchronous generator/motor is shown in Fig. 2. Consider the following assumptions: the magnetic circuits are considered linear, and also balanced armature currents and the rotor has no damping windings.

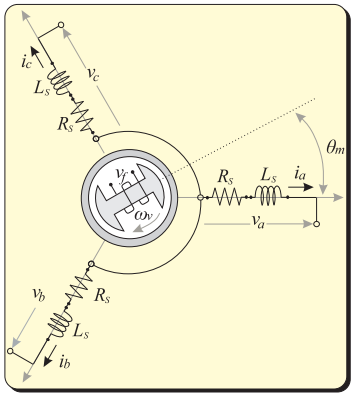

Figure 2: Schematic synchronous generator (being $p = 1$).

The flux linkages of the armature phases a, b and c and the field winding f are expressed in terms of inductances and currents, such as:

$$\Phi_a = L_{aa}i_a + L_{ab}i_b + L_{ac}i_c + L_{af}i_f \quad (1)$$
$$\Phi_b = L_{ba}i_a + L_{bb}i_b + L_{bc}i_c + L_{bf}i_f \quad (2)$$
$$\Phi_c = L_{ca}i_a + L_{cb}i_b + L_{cc}i_c + L_{cf}i_f \quad (3)$$
$$\Phi_f = L_{af}i_a + L_{bf}i_b + L_{cf}i_c + L_{ff}i_f. \quad (4)$$

The items above subscripted with equal letters (L_{xx}) indicate self-inductances and the ones with different letters (L_{xy}) indicate mutual inductance between two windings. Being i_a, i_b and i_c the phase currents of the stator and i_f the excitation current.

The mutual inductances between stator and rotor vary instantaneously with θ_m, which is the virtual mechanical angle between the axis of the field winding and the phase a, as it is shown in Fig. 2. In order to obtain the mutual inductance, it is necessary to calculate the electric angle between the magnetic axis of the field winding and the phase a, which is given

by $\theta_v = p\theta_m$. Where θ_v is the virtual electric angle and p is the number of pole pairs, thus:

$$L_{af} = M_f \cos(\theta_v) \tag{5}$$
$$L_{bf} = M_f \cos(\theta_v - \tfrac{2\pi}{3}) \tag{6}$$
$$L_{cf} = M_f \cos(\theta_v - \tfrac{4\pi}{3}). \tag{7}$$

For a synchronous machine as a cylindrical rotor, the self-inductances of the stator and rotor windings do not depend on θ_v. Then, the self-inductances are constant. Therefore:

$$L_{aa} = L_{bb} = L_{cc} = L_{aac} + L_{aad} \tag{8}$$
$$L_{ff} = L_{ffc} + L_{ffd}. \tag{9}$$

Where L_{aac} and L_{ffc} are the components of the self-inductances due to the main fluxes of the stator windings and field. So, L_{aad} and L_{ffd} are the additional components due to the leakage flux [4].

The mutual inductances of the armature windings are related directly to the main flux. As the armature windings are displaced by 120° electric and as $\cos(120°) = -1/2$, then:

$$L_{ab} = L_{ba} = L_{ac} = L_{ca} = L_{bc} = L_{cb} = -\frac{1}{2}L_{aac}. \tag{10}$$

Replacing (8) and (10) in the expression of the flux linkages of phase a for (1), then:

$$\Phi_a = (L_{aac} + L_{aad})i_a - \frac{1}{2}L_{aac}(i_b + i_c) + L_{af}i_f. \tag{11}$$

As the armature currents are balanced, then:

$$i_a + i_b + i_c = 0 \tag{12}$$
$$i_b + i_c = -i_a. \tag{13}$$

Then replacing in (11), thus:

$$\Phi_a = (\frac{3}{2}L_{aac} + L_{aad})i_a + L_{af}i_f. \tag{14}$$

By categorizing $\frac{3}{2}L_{aac} + L_{aad}$ as a synchronous inductance (L_s), it is concluded that:

$$\Phi_a = L_s i_a + L_{af} i_f. \tag{15}$$

Doing the same for all other phases of the armature winding and setting:

$$\vec{\Phi}_{abc} = \begin{bmatrix}\Phi_a \\ \Phi_b \\ \Phi_c\end{bmatrix}, \widetilde{cos}(\theta_v) = \begin{bmatrix}\cos(\theta_v) \\ \cos(\theta_v - \frac{2\pi}{3}) \\ \cos(\theta_v - \frac{4\pi}{3})\end{bmatrix},$$

$$\vec{i}_{abc} = \begin{bmatrix}i_a \\ i_b \\ i_c\end{bmatrix}, \widetilde{sen}(\theta_v) = \begin{bmatrix}sen(\theta_v) \\ sen(\theta_v - \frac{2\pi}{3}) \\ sen(\theta_v - \frac{4\pi}{3})\end{bmatrix}.$$

Therefore, the flux stator and rotor can be rewritten as:

$$\vec{\Phi}_{abc} = L_s\vec{i}_{abc} + M_f i_f \widetilde{cos}(\theta_v) \tag{16}$$

$$\Phi_f = L_f i_f + M_f \left\langle \vec{i}_{abc}, \widetilde{cos}(\theta_v) \right\rangle. \tag{17}$$

Assuming that the stator winding resistance is R_s, then the voltages at the stator terminals of the synchronous generator, are given by $\vec{v}_{abc} = \begin{bmatrix}v_a & v_b & v_c\end{bmatrix}^T$ and they can be obtained by summing the voltage drops in the resistor R_s and the induced voltage. In this context, the induced voltages can be calculated by Faraday's law using (16), thus:

$$\vec{v}_{abc} = -R_s\vec{i}_{abc} - \frac{d\vec{\Phi}_{abc}}{dt} = -R_s\vec{i}_{abc} - L_s\frac{d\vec{i}_{abc}}{dt} + \vec{e}_{abc} \tag{18}$$

where $\vec{e}_{abc} = \begin{bmatrix}e_a & e_b & e_c\end{bmatrix}^T$ represents the back electromotive force (EMF). The vector $\vec{e}_{abc}$ is given by:

$$\vec{e}_{abc} = M_f \frac{d[i_f \widetilde{cos}(\theta_v)]}{dt} = M_f i_f \omega_v \widetilde{sen}(\theta_v) + M_f \frac{di_f}{dt}\widetilde{cos}(\theta_v). \tag{19}$$

Considering a constant excitation current ($\frac{di_f}{dt} = 0$) and $\Phi_v = M_f i_f$ as virtual air gap flux of the Synchronverter. Thus:

$$\vec{e}_{abc} = \Phi_v \omega_v \widetilde{sen}(\theta_v). \tag{20}$$

Similarly, as it occurred in (18), the voltages at the terminals of the field winding are calculated as it follows:

$$v_f = -R_f i_f - \frac{d\Phi_f}{dt} \tag{21}$$

where R_f is the resistance of the rotor windings.

2.1.2. Mechanical Model

The mechanical model of the virtual synchronous machine is associated with the swing equation of the conventional synchronous machine, thus:

$$J\frac{d\omega_v}{dt} = T_m - T_e - D_p\omega_v. \tag{22}$$

Where J is the moment of inertia of all the rotating parts with the rotor, T_m is the mechanical torque, T_e is the electromagnetic torque, and D_p is the damping factor.

2.2. Power Circuit

In the power circuit, there is the VSI, which consists of 6 (six) IGBTs (Insulated Gate Bipolar Transistor), being two per each one of the three legs. The switches of a leg cannot be triggered simultaneously. It also consists of a three-phase LC filter, which is used to attenuate switching ripple, where the resistance R_s and the inductance L_s represent the impedance of the armature windings of the virtual synchronous generator, and L_g and R_g are parameters of the grid. The power circuit is represented in Fig. 3, according to (18).

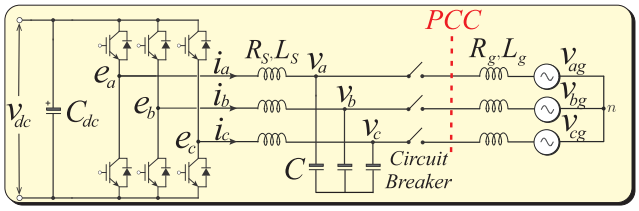

Figure 3: Power circuit of Synchronverter.

3. Lithium-Ion BESS Modeling

Lithium-Ion battery was used in this work due to high energy density and its massive use by RES. There are several models to represent a lithium-ion battery. In [1], tests were performed on a completely new 20Ah $LiFePO_4$ cell. The intuition of the test was to obtain an analytical model based on the interpolation of data obtained in the field that related the hysteresis between state-of-charge (SoC) and open circuit voltage (V_{oc}) of battery. Therefore, with the set of cells obtained from this model, it is possible to analyze the nonlinear behavior of the voltage during the loading and unloading of the battery bank. In this work the effect of hysteresis was disregarded, it was considered an intermediate curve that the loading and unloading of the battery.

To integrate with the simulated environment, the battery bank is represented as an equivalent circuit model, which consists of an ideal voltage source (V_{bat}), as shown in Fig. 4. The estimation of the SoC of the battery bank was made according to [9].

$$SoC(k+1) = SoC(k) - \frac{\Delta k \begin{cases} \frac{1}{\eta_d} p(k) & \text{if } p(k) > 0, \\ \eta_c p(k) & otherwise \end{cases}}{E_{bat}}, \quad (23)$$

where E_{bat} is the energy capacity, η_c and η_d are charging and discharging efficiencies. These data are sampled with a time step, Δk. It defines $p(k)$ to be the power requested from ($p(k)$ positive) or sent to ($p(k)$ negative) the storage unit at the specific time.

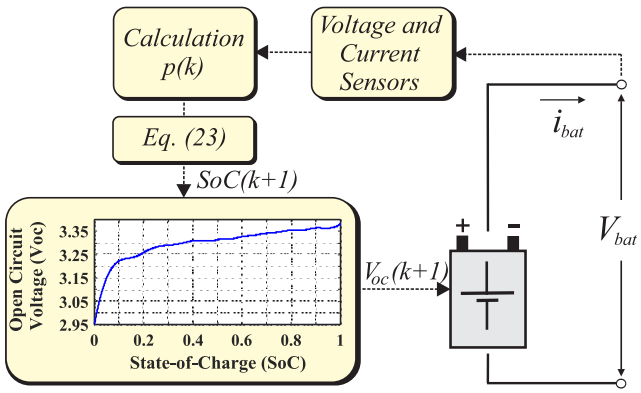

Figure 4: Real model of lithium-ion battery.

4. Operation Modes of Synchronverter

The block diagram of the Synchronverter control, as shown in Fig. 5, can be implemented via software and was based on the equations in Section II. Therefore, the VSI operates similarly to the SG, so that variations in amplitude (E) and phase (θ_v) of its terminal voltage adjust active and reactive power delivered to the grid. Reference voltage (E^*_{abc}) is imposed by VSI.

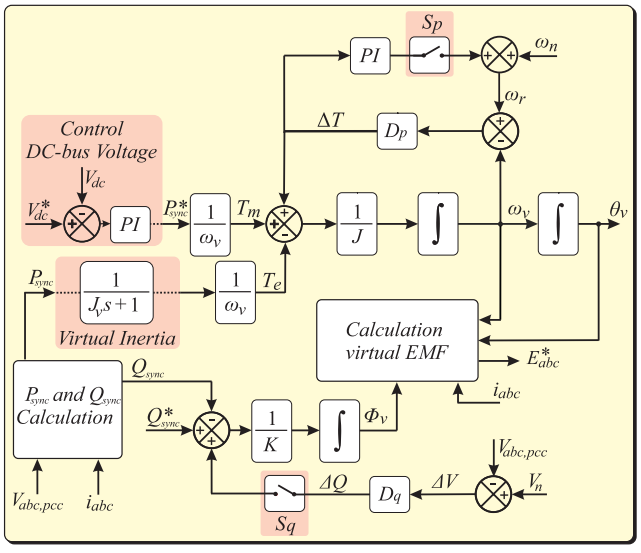

Figure 5: Block diagram of the control of the Synchronverter.

4.1. Frequency Drooping and Regulation of Active Power

The active power regulation mechanism in the Synchronverter has a cascade control structure where the internal loop represents the frequency control (angular velocity) and the external loop indicates the active power control. It is related to the SG mechanical model, as it is seen in (22).

The frequency control action is defined by the position of the switch S_p. When S_p turns off, the frequency-droop

mechanism is implemented in a Synchronverter by comparing the virtual angular speed (ω_v) with the angular frequency reference (ω_r) (is usually equal to the nominal angular frequency of the grid (ω_n)) and adding this difference, multiplied with a gain (D_p), generating a ΔT that will be added the active torque T_m. However, the damping factor (D_p) actually behaves as the frequency droop coefficient, which is defined as the radio of the required change of torque ΔT to the change of angular speed ($\Delta\omega$). therefore:

$$D_p = \frac{\Delta T}{\Delta \omega}. \tag{24}$$

Thus, when S_p is turned on, ΔT is controlled to be 0 in the steady state via the PI controller. Hence, T_e is the same as T_m, which results in $P^*_{sync} = P_{sync}$ [23].

4.2. Voltage Drooping and Regulation of Reactive Power

The idea of the Synchronverter voltage regulator is similar to that used by the conventional SG. With S_q turned on, the difference between the reference voltage (V_n) and the $V_{abc,pcc}$ – values in RMS – is the voltage amplitude tracking error (ΔV). This error is multiplied by the voltage-drooping coefficient (D_q) and then added to the tracking error between the reference value (Q^*_{sync}) and the measured reactive power (Q_{sync}). The resulting signal is then fed into an integrator with a gain of $1/K$ to generate virtual flux (ϕ_v), calculating EMF [22]. For S_q to turn off, ϕ_v will have a constant value in the steady state regardless of the voltage difference between V_n and $V_{abc,pcc}$, thus $Q^*_{sync} = Q_{sync}$.

4.3. Synthetic Inertia

The moment of inertia (J) in the Synchronverter is not associated with the inertia, but with a control parameter. Then, a configurable inertial time constant is introduced by adding a low-pass filter to the measured active power (P_{sync}) signal, according to Fig. 5; where J_v is the virtual inertia time constant required, increasing the virtual inertia J_v indeed slows the frequency response down [24].

4.4. Control the DC-bus voltage

The active reference power may be set by controlling the DC-bus voltage, concept similar to dq control, where the error between the measured voltage (V_{dc}) and its reference (V^*_{dc}) is entered in the PI controller to generate the P^*_{sync}. Therefore, S_p is turned on.

5. Simulation Results

The system has been implemented in MATLAB Simulink, the solver used in the simulations is ode23tb, where the essential system parameters are described on the Table 1 (the base values used were $V_b = 690\,\text{V}$ e $S_b = 500\,\text{kVA}$).

The battery bank was dimensioned to compensate a 450 kW power during one hour. Therefore, it is composed by 20 sets of 346 batteries in series (the sum of the voltages of the batteries close to the nominal voltage of the DC-bus). The battery data was obtained in [8].

Table 1
Parameters Used in Simulation.

Parameter	Value	Parameter	Value
L_s	0.0031 pu	R_s	0.0094 pu
C	0.105 pu	L_g	0.0001 pu
R_g	0.105 pu	f_{ch}	10 kHz
V_g, V_n	690 V_{rms}	f_g, f_n	50 Hz
$Z_{sc,\phi 3}$	0.1 mΩ	D_p	35 N.m/(rad/s)
D_q	0.5 kvar/V	K	10 kvar/V
$k_{p,V_{dc}}$ / $k_{i,V_{dc}}$	100 / 300	$k_{p,\Delta T}$ / $k_{i,\Delta T}$	0.1 / 1
J_v	0.1 / 0.01	C_{dc} / V^*_{dc}	100 mF/1150 V
Bat. cathode	$LiFePO_4$	Bat. anode	Graphite
$E_{bat,n}$	65 Wh	$V_{bat,n}$	3.3 V
$I_{bat,max}$	300 A	R_{bat}	0.5 Ω

The simulation was started with $P^*_{sync} = 0$ and $Q^*_{sync} = 0$, with the switches S_p turned on and S_q turned off. During 0.5 s the Synchronverter gets self-synchronized with the grid. To test all the operation modes of Synchronverter in controlling the BESS, mainly charge-discharge control through the conventional grid-side control, the following scenarios were simulated: active power controlled from DC-bus voltage; symmetrical faults; frequency support and regulation of active power; and voltage support and regulation of reactive power.

5.1. Scenario A – Active power controlled from DC-bus voltage

In this scenario the behavior of the Synchronverter is analyzed with P^*_{sync} controlled from the DC-bus voltage error, similar to the conventional grid-side control. Variations of active power in VSI-I to 270 kW at 2 s, −130 kW at 2.5 s and 70 kW at 3.5 s were simulated. Fig. 6 shows that VSI-II follows the active power variations and maintains the DC-bus voltage at its reference value. Thus, it is observed that the Synchronverter is capable of acting similarly to conventional control, with reference to the active power delivered/consumed to the mains via DC bus voltage control.

The same power variations in VSI-I were simulated for different virtual inertia J_v and frequency responses of the Synchronverter are shown in Fig. 6. The system responses obtained different transient duration times, where increasing J_v indeed slows the frequency response down.

For the curves of LC filter currents it is observed that a transition from generator to motor occurs right after 3.5 s. The opposite transition, from motor to generator, occurred right after 2.5 s.

5.2. Scenario B – Symmetrical faults

To implement the fault scenario symmetrical fault was applied to the PCC in order to reproduce real grid voltage sag 100% conditions with 100 ms duration, as specified in the grid code requirements. This scenario aims to verify the robustness of the Synchronverter against a symmetrical fault, the reference of P^*_{sync} was kept via the DC-bus voltage control and with the voltage droop enable.

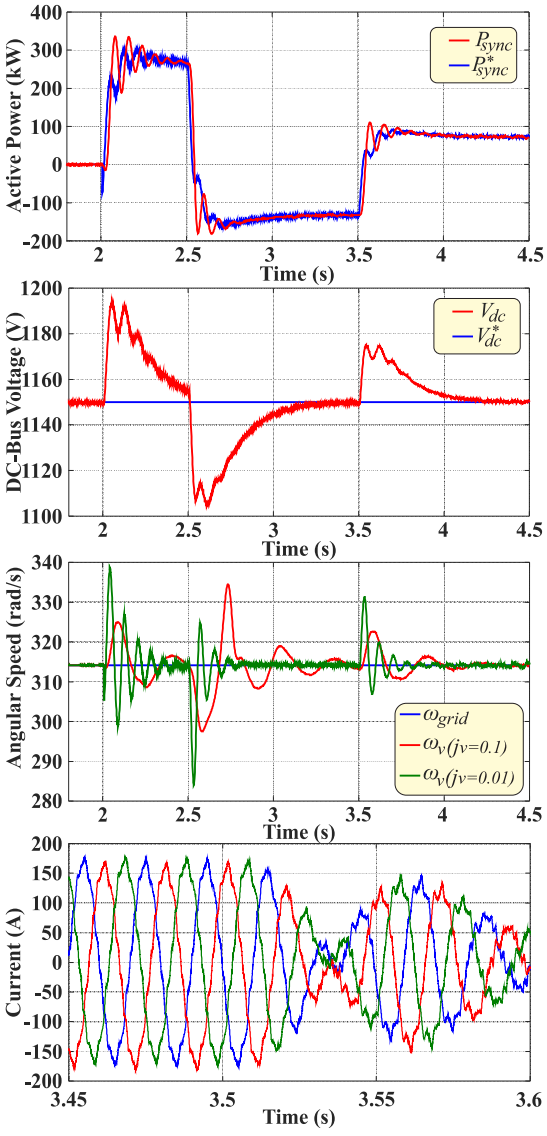

Figure 6: Scenario A – Active power of Synchronverter controlled via DC-bus voltage.

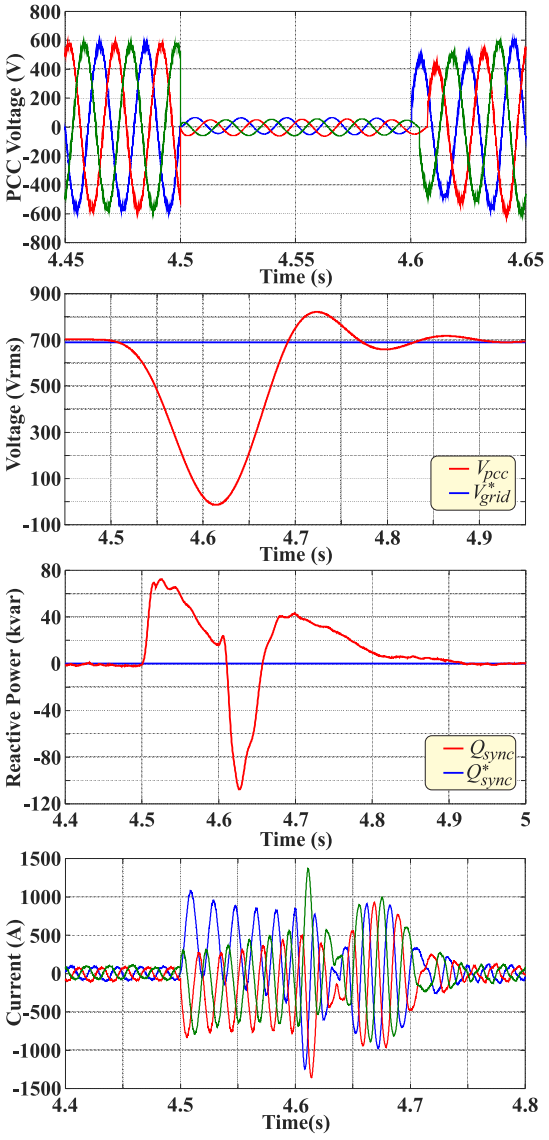

Figure 7: Scenario B – Voltage support at the time of symmetrical fault.

At $t = 4.5$ s the fault was applied, as shown in Fig. 7. The high current levels at the fault interval are related to the input of reactive power to maintain voltage stability in the PCC. Proving the effectiveness of the Synchronverter voltage control, preventing the grid from losing voltage stability.

This demonstrates the robustness of the Synchronverter, being able to withstand high levels of voltage sag.

5.3. Scenario C – Frequency support and Regulation of Active Power

At $t = 5$ s the grid frequency was abruptly reduced to 49 Hz, that is 2% lower than the nominal one, at $t = 6$ s the frequency has been reestablished to its nominal value. The Synchronverter automatically detects the grid frequency variation, then connects the battery bank in parallel to the DC-bus. The frequency droop coefficient is chosen as $D_p = 35$ so that the frequency drops 1% when the torque (power) increases 35%. The droop mechanism is enabled automatically along with the battery bank, when the grid frequency increases the active power decreases, when the grid frequency decreases the active power increases. This action is very important for maintaining grid frequency stability. Then, after the droop mechanism was enabled at $t = 5$ s, the synchronverter increased the active power output by 70 kW, that is 70% ot the rated power, corresponding to 2% drop ot the frequency, as shown in Fig. 8.

After active power supplying from 5s to 6s battery bank discharges, consequently reducing its voltage and *SoC*. After establishing the frequency at its nominal value, it was necessary to charge the batteries. At $t = 6.62$ s the active power reference value was set to $P^*_{sync} = -400$ kW. Thus, it was possible to charge the batteries increasing both voltage and *SoC*.

Moreover, the inertia time constant can be reconfigured

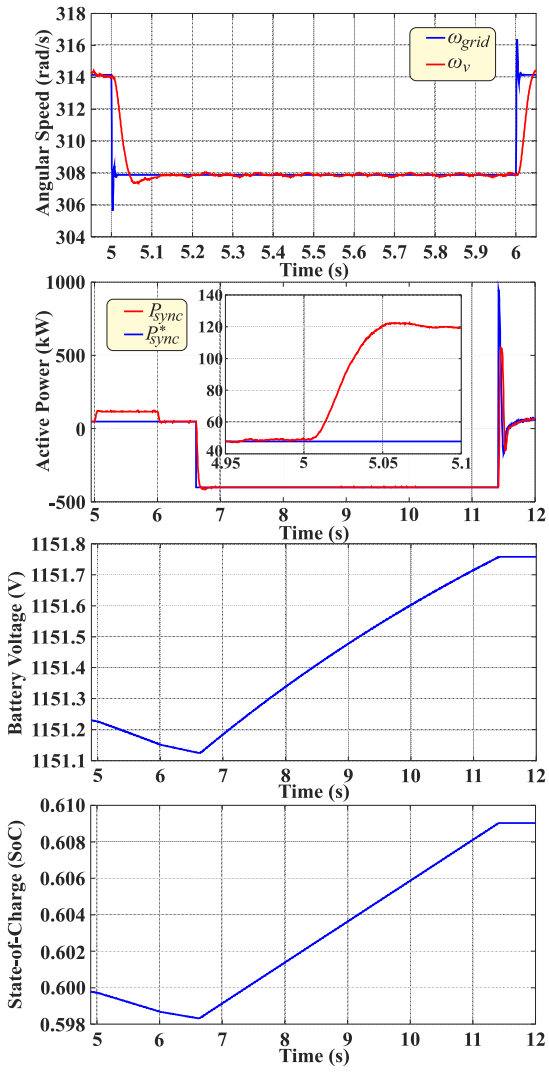

Figure 8: Scenario C – Frequency support and charge/discharge of the battery bank.

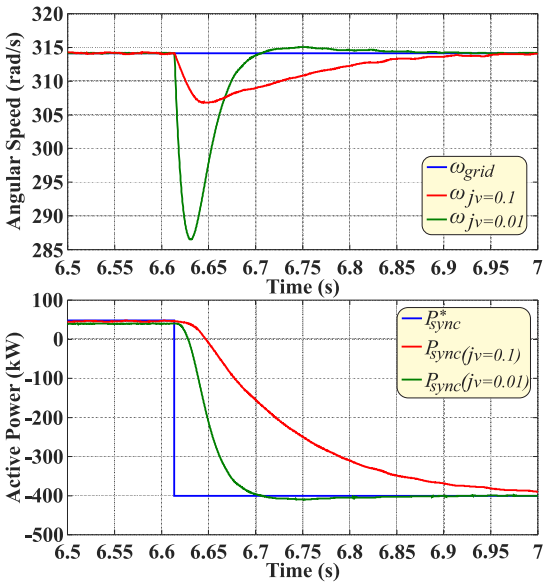

Figure 9: Scenario C – The frequency responses of the Synchronverter with different virtual inertia.

to achieve the desired speed of frequency response. This change of frequency response is possible via the control algorithm.

As can be seen in Fig. 9, at $t = 6.62$ s an abrupt variation in power was caused, so it is possible to observe the behavior of active power and angular velocity (frequency) with different virtual inertia.

The frequency response behaves as expected: increasing the virtual inertia J_v indeed slows the frequency response down and with a slower variation in active power. On the other hand, by decreasing the value of J_v the frequency response will be faster, and consequently, the active power variation too.

5.4. Scenario D – Voltage support and Regulation of Reactive Power

In this scenario, the grid voltage initially is 690 V, then, voltage variations are simulated in the grid. In the interval from $t = 13$ s to $t = 14$ s there is a voltage variation to 710 V, and from $t = 15$ s to $t = 16$ s to 670 V, according to Fig.10. In this case, there is no variation in grid frequency.

Initially voltage droop is enabled providing voltage support to the grid at $t = 13$ s. The grid voltage increases while the reactive power delivered by Synchronverter decreases automatically, acting in the maintenance of voltage stability of the grid.

At $t = 14$ s, the voltage is restored and voltage droop was disabled. Therefore, voltage variations in the grid do not affect the reactive power delivered by the Synchronverter. For this specific scenario, there is no need to use the battery bank since the reactive power does not affect the DC-bus voltage.

6. Conclusions

This paper investigated the potential use of Synchronverter to control $LiFePO_4$ battery connected to DC-bus of distributed generation. It has been illustrated that this approach may enable high integration of renewable energy sources into the grid. Due to its autonomous operation, it is possible to attenuate grid disturbances. The simulation results show that lithium-ion battery bank with Synchronverter is able to provide grid voltage and frequency supports, just as it is also possible to obtain greater control of active and reactive power delivered to grid. Also, it is able to obtain synthetic inertia, therewith the frequency responses of the Synchronverter are different during the transient process because of the different virtual inertia. This mitigate the trend of decreasing inertia due to the penetration of renewable energy sources into the grid. Finally, it was observed there is no need to use a DC/DC converter to control battery charge-discharge propitiating to reduce system complexity and cost.

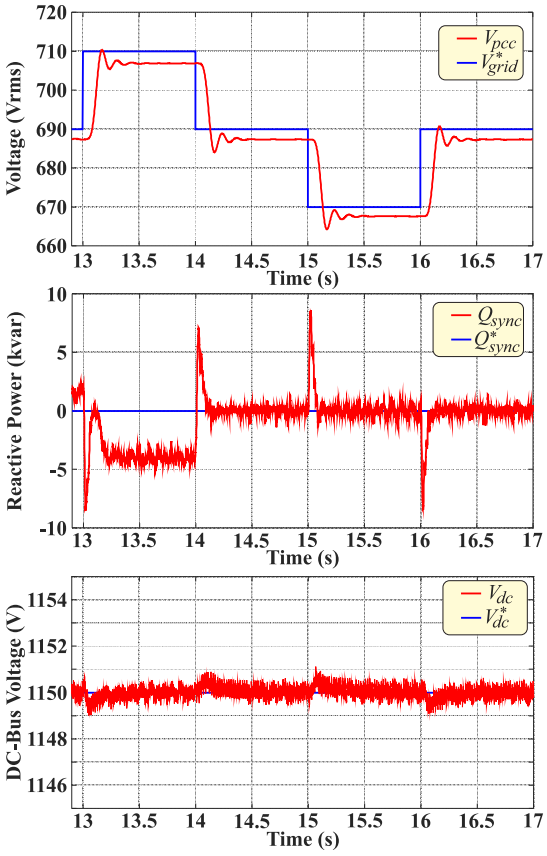

Figure 10: Scenario D – Voltage support and regulation of reactive power.

7. Acknowledgment

This work was supported by the National Council for Scientific and Technological Development (CNPq) and by the Coordination for the Improvement of Higher Education Personnel (CAPES), Brazil.

References

[1] Baronti, F., Zamboni, W., Femia, N., Roncella, R., Saletti, R., 2013. Experimental analysis of open-circuit voltage hysteresis in lithium-iron-phosphate batteries, in: IEEE Industrial Electronics Society, pp. 6728–6733. doi:10.1109/IECON.2013.6700246.

[2] Beck, H.P., Hesse, R., 2007. Virtual synchronous machine, in: Electrical Power Quality and Utilisation, pp. 1–7.

[3] Chen, Y., Hesse, R., Turschner, D., H. Beck, 2007. Comparison of methods for implementing virtual synchronous machine on inverters, in: Renewable energy e power quality journa, pp. 734–739.

[4] Fitzgerald, A.E., Kingsley, C., 2003. Electric Machinery. Mc Graw Hill.

[5] Jia Liu, Miura, Y., Ise, T., 2014. Dynamic characteristics and stability comparisons between virtual synchronous generator and droop control in inverter-based distributed generators, in: International Power Electronics Conference, pp. 1536–1543. doi:10.1109/IPEC.2014.6869789.

[6] Karapanos, V., Yuan, Z., Haan, S., Visscher, K., 2011. A control algorithm for the coordination of multiple virtual synchronous generator units.

[7] Liu, Y., Hao, M., He, Y., Zang, C., Zeng, P., 2019. Review and applications of virtual synchronous machines technologies, in: IEEE Innovative Smart Grid Technologies, pp. 593–598. doi:10.1109/ISGT-Asia.2019.8881466.

[8] Mathewson, S., 2014. Experimental Measurements of LiFePO4 Battery Thermal Characteristics. Ph.D. thesis. University of Waterloo.

[9] Mégel, O., Mathieu, J.L., Andersson, G., 2013. Maximizing the potential of energy storage to provide fast frequency control, in: IEEE PES ISGT Europe 2013, pp. 1–5. doi:10.1109/ISGTEurope.2013.6695380.

[10] Pholboon, S., Sumner, M., Ierna, R., 2019. Virtual synchronous machine control for grid transmission compliance studies, in: International Conference on Smart Energy Systems and Technologies, pp. 1–5. doi:10.1109/SEST.2019.8849041.

[11] Saadatmand, S., Shamsi, P., Ferdowsi, M., 2021. Power and frequency regulation of synchronverters using a model free neural network-based predictive controller. IEEE Transactions on Industrial Electronics 68, 3662–3671. doi:10.1109/TIE.2020.2984419.

[12] Sakimoto, K., Miura, Y., Ise, T., 2011. Stabilization of a power system with a distributed generator by a virtual synchronous generator function, in: 8th International Conference on Power Electronics - ECCE Asia, pp. 1498–1505. doi:10.1109/ICPE.2011.5944492.

[13] Sharma, N., Buwa, O.N., Thakre, M.P., 2020. Dynamic phasor modeling of single phase roof top pv with synchronverter control, in: 2020 Third International Conference on Advances in Electronics, Computers and Communications (ICAECC), pp. 1–6. doi:10.1109/ICAECC50550.2020.9339528.

[14] Silva Jr, G.P., Barros, L.S., 2019. Using synchronverter in distributed generation for frequency and voltage grid support, in: 2019 IEEE 15th Brazilian Power Electronics Conference and 5th IEEE Southern Power Electronics Conference (COBEP/SPEC), pp. 1–6. doi:10.1109/COBEP/SPEC44138.2019.9065482.

[15] Silva Junior, G.P., Barros, L.S., 2019. Synchronverter operation in active and reactive support mode, in: 2019 Workshop on Communication Networks and Power Systems (WCNPS), pp. 1–5. doi:10.1109/WCNPS.2019.8896239.

[16] Silva Junior, G.P., Barros, L.S., 2020. Analysis of synchronverter utilization in conventional grid side control of distributed generation based on full power converter, in: Automatic Brazilian Congress.

[17] Silva Junior, G.P., Nascimento, T.F., Barros, L.S., 2020. Comparison of virtual synchronous generator strategies for control of distributed energy sources and power system stability improvement, in: Brazilian Symposium on Electrical Systems, pp. 1–5.

[18] Van, T.V., Visscher, K., Diaz, J., Karapanos, V., Woyte, A., Albu, M., Bozelie, J., Loix, T., Federenciuc, D., 2010. Virtual synchronous generator: An element of future grids, in: Innovative Smart Grid Technologies Conference Europe (ISGT Europe), pp. 1–7. doi:10.1109/ISGTEUROPE.2010.5638946.

[19] Yaramasu, V., Wu, B., 2017. Model Predictive Control of Wind Energy Conversion Sistem. John Wiley & Sons, Ltd.

[20] Yi, Z., Dong, W., Etemadi, A.H., 2018. A unified control and power management scheme for pv-battery-based hybrid microgrids for both grid-connected and islanded modes. IEEE Transactions on Smart Grid 9, 5975–5985. doi:10.1109/TSG.2017.2700332.

[21] Zhong, Q., Nguyen, P., Ma, Z., Sheng, W., 2014. Self-synchronized synchronverters: Inverters without a dedicated synchronization unit. IEEE Transactions on Power Electronics 29, 617–630. doi:10.1109/TPEL.2013.2258684.

[22] Zhong, Q., Weiss, G., 2011. Synchronverters: Inverters that mimic synchronous generators. IEEE Transactions on Industrial Electronics 58, 1259–1267. doi:10.1109/TIE.2010.2048839.

[23] Zhong, Q.C., 2016. Virtual synchronous machines - a unified interface for smart grid integration, in: IEEE Power Electronics Magazine, pp. 1–7.

[24] Zhong, Q.C., 2020. Power Electronics Enables Autonomous Power Systems. John Wiley & Sons, Ltd.